University of Oslo

FYS4505

Methods and Instrumentation for Nuclear and Particle Physics

Report 1: NaI[Tl] Detector Characteristics

Author:
Håkon Fossheim

October 2, 2020

We perform χ^2 fits of the all peaks in the data sample obtained from a ^{137}Cs source over a data acquisition period of 600 sec by use of a Thallium activated NaI detector. From the fitted photopeak, the energy of the γ-rays produced by the decay product of ^{137}Cs was found to be $E_\gamma = 662.4\,\text{keV} \pm 0.0\,\text{keV}$. Furthermore, the fitted Compton edge gave an estimate of $m_e = 590.0\,\text{keV} \pm 17.1\,\text{keV}$ for the electron mass in Natural units.

The resolution of these peaks were found to be $R_{\text{photopeak}} = 7.72\,\text{keV} \pm 0.02\,\text{keV}$ and $R_{\text{Compton edge}} = 30.1\,\text{keV} \pm 0.02\,\text{keV}$.

I. Introduction

As the radionuclide $^{137}_{55}$Cs decays through β^- decay, we are left with a metastable state of Barium, namely $^{137m}_{56}$Ba. As this metastable state transitions to the $^{137}_{56}$Ba groundstate, a 662 keV γ-ray is emitted from the nucleus.

In this experiment, we used a 2x2 inch NaI(Tl) crystal was to detect these gamma-rays. As a gamma ray enters the detector, it causes ionization in the sodium iodide crystal. This creates excited states which get de-excited through the emission of photons. This process is known as scintillation, and detectors based on this principle are called scintillation detectors. In a pure NaI crystal, electrons excited by the primary γ-rays could re-emit this photon through recombination. This photon would then have sufficient energy to ionize another atom, making the NaI crystal opaque to these photons.

By doping the crystal with Thallium, we introduce *activator states* between the valence- and conduction band. The free electron can then de-excite to these states and in the process emit photons of lower frequency which are transparent to the crystal.

The crystal is enclosed in a reflective material. The purpose of this is twofold; to increase the efficiency of the detector as well as to prevent the crystal from absorbing moisture from the surrounding air. [mention the two types of reflectors that can be used].

The amount of electrons emitted from the photocathode for a single incoming gamma ray is far too low to be able to detect with our instruments. A photomulti-

plier tube is therefore used to amplify the signal. This is depicted in Fig.(1).

The photomultiplier tube consists of a series of dynodes biased to consecutively higher voltages. As an electron strikes the first dynode, the positive voltage of the dynode allows it to free more electrons, which go on to strike the second dynode. This creates an electron cascade which by the time it reaches the anode will constitute a significant signal. The photomultiplier is contained in a vacuum tube to allow free pathing of these electrons.

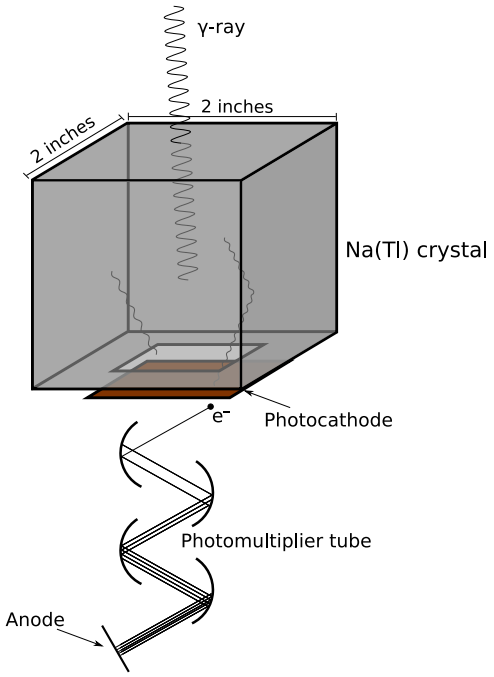

FIG. (1)

The anode is connected to the a preamplifier, which in our case is built into the detector. Scintillation detectors in general produce a very good signal yield, and so in our case its primary purpose is to provide a more favorable RC time constant when connected to the linear amplifier. The linear amplifier allows for shaping of the signal peaks, reducing so-called *pile-up*. This occurs when two or more signal peaks overlap to such an extent that they are counted as a single event. The width of the signal after shaping is referred to as *shaping time*, and has a lower limit which is determined by the inherent resolution of the detector.

II. Theory

A. Peak Resolution

In an ideal world with no uncertainties in our measurements, a given process would produce a delta function at the energy of the gamma ray produced by said process. However, some uncertainties are inevitable, and in most cases this leads to a smearing of our signal which in the vast majority of cases manifests itself as a Gaussian distribution due to the central limit theorem. The functional form of this Gaussian is then

$$f(x) = f_{max} \exp\left\{-\frac{(x-\mu)^2}{2\sigma^2}\right\} \tag{1}$$

Where E is the energy of the gamma ray produced by our process.

The resolution of this Gaussian peak is given by

$$R = \frac{FWHM}{E} \tag{2}$$

And is a measures of how "delta-like" our the peak is. Here FWHM is the full width at half maximum, namely the width of the distribution at $f(x) = f_{max}/2$. $E = \mu$ is the mean of the Gaussian, and is the energy of the process in question[1]. We see that the resolution decreases with energy. A depiction of the mentioned quantities is given in Fig.(2).

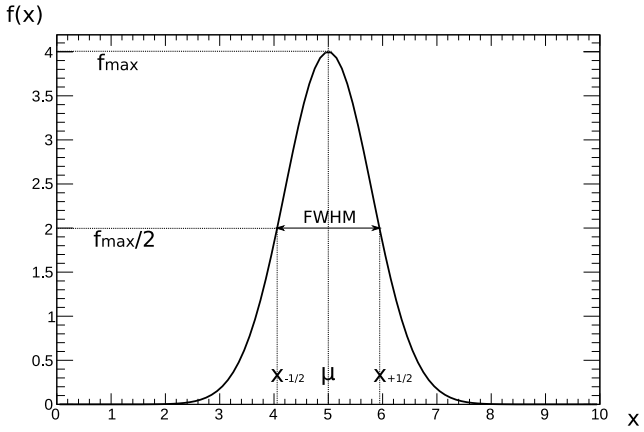

FIG. (2)

Let $x_{-\frac{1}{2}}$ and $x_{+\frac{1}{2}}$ denote the two solutions to $f(x) = \frac{1}{2} f_{max}$. We then have

$$f(x_{\pm\frac{1}{2}}) = \frac{1}{2} f_{max} = f_{max} \exp\left\{-\frac{(FWHM/2)^2}{2\sigma^2}\right\} \tag{3}$$

Taking the logarithm of both sides yields

$$\ln\frac{1}{2} = -\frac{FWHM^2}{8\sigma^2}$$
$$\Rightarrow FWHM = \sigma\sqrt{-8\ln(1/2)} \approx 2.35\sigma \tag{4}$$

[1] In the case of no uncertainties.

We may therefore rewrite the resolution in terms of the standard deviation of our Gaussian peak;

$$R = \frac{FWHM}{E} \approx \frac{2.35\sigma}{E} \tag{5}$$

This will come in handy, as the standard deviation will be easily accessible after performing fits of the various peaks in our data.

B. Multi Channel Analyzer

The multichannel analyzer (MCA) discretizes our signal. A relevant energy range is split up into a number of *channels* of specific widths, ΔE. This number will be a power of two, and in our case we had $2^{11} = 2048$ channels.

As time passes, bins corresponding to the height of the passing peak will be incremented. This is illustrated in Fig.(3). Here we have depicted two different processes. In an ideal world where a given process always results in the exact same pulse-height, this process would only ever land in one bin. However, since the energy and thereby the channel number of the pulse height are subject to fluctuations stemming from uncertainties in our instruments, a given process will be Gaussian distributed around the bin corresponding to the true energy.

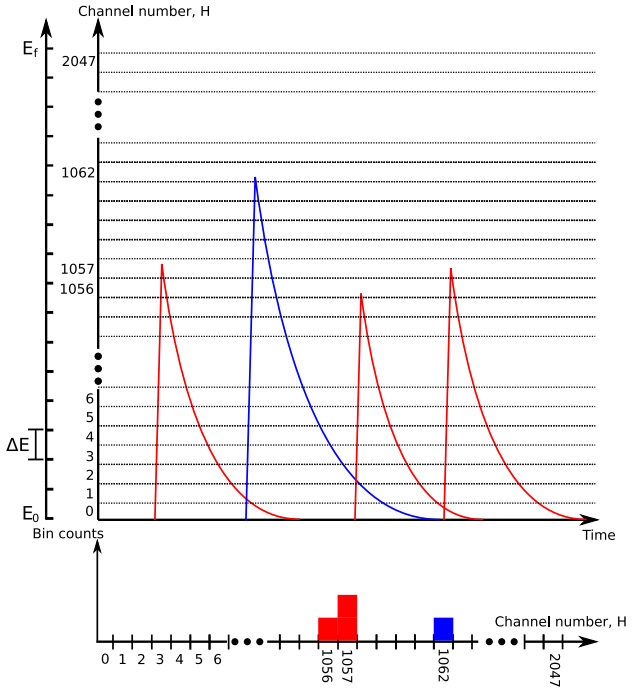

FIG. (3) Illustration of how the MCA works. Signal pulses of two separate processes are depicted in blue and red. Note that this figure is not meant to be accurate, and in reality we would likely have a greater separation in H between two processes.

The output of the MCA will thus be a histogram with bins corresponding to channel numbers. To convert this [2] to an energy spectrum, we therefore need to convert from channel numbers,H, to energy, E. As seen in Fig.(3), the energy axis will have an offset E_0 and a stretching factor ΔE relative to the channel axis, and thus

$$E(H) = E_0 + (\Delta E)H \tag{6}$$

E_0 and ΔE are our *calibration coefficients*, and were found to be $E_0 = 6.644839$ and $\Delta E = 1.220401$.

C. Efficiency

The efficiency of a detector is simply the fraction of events that it detects

$$\epsilon = \frac{\text{Number of events detected}}{\text{Number of actual events}} \tag{7}$$

As will be discussed in Sec.(IV B), the efficiency of a scintillation detector increases with the size of the crystal. This is because fewer secondary γ-rays escape through the surfaces of the crystal. Likewise, for a fixed detector size, the efficiency should decrease as we increase the energy of the primary γ-ray, since this increases the mean free path of the secondary rays, thereby allowing more of them to escape the detector.

D. Error propagation

For a function f of two independent variable x and y, the error on f will be given by[2]

$$(\Delta f[x,y])^2 \approx (\Delta x)^2 \left(\frac{\partial f}{\partial x}[x,y]\right)^2 + (\Delta y)^2 \left(\frac{\partial f}{\partial y}[x,y]\right)^2 \tag{8}$$

Where the approximation stems from ignoring higher order terms in the Taylor expansion of f around (x, y).

III. Methods

We first analyze the pulse signal by connecting the oscilloscope directly to the inbuilt preamplifier of the NaI detector. The resulting signal pulse can be seen in Fig(4).

[2] In our case by use of ROOT

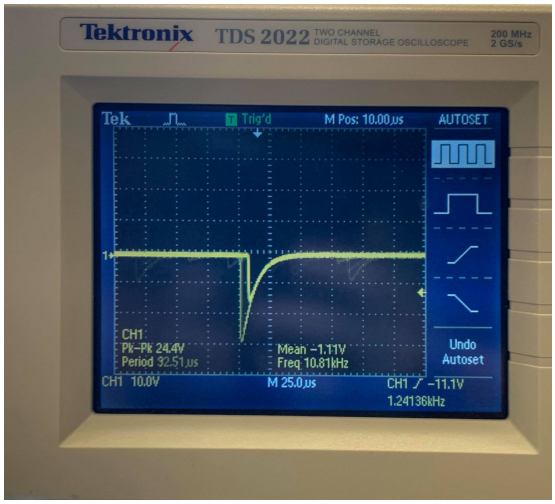

FIG. (4) Pulse signal output when connecting our oscilloscope (Tektronix TDS2022) directly to the inbuilt preamplifier of the NaI detector.

As seen, the resulting signal has a negative voltage. This is due to the collection of negative charges at the anode.

Next, we send the signal through the linear amplifier before observing it in the oscilloscope. We adjust the resolution by setting the coarse gain to 5, the peaking time to 1μs and shaping time to 0.05. The resolution will not increase by reducing this number any further, due to the inherent resolution of the detector.

The inverted pulse signal is shown in Fig.(5).

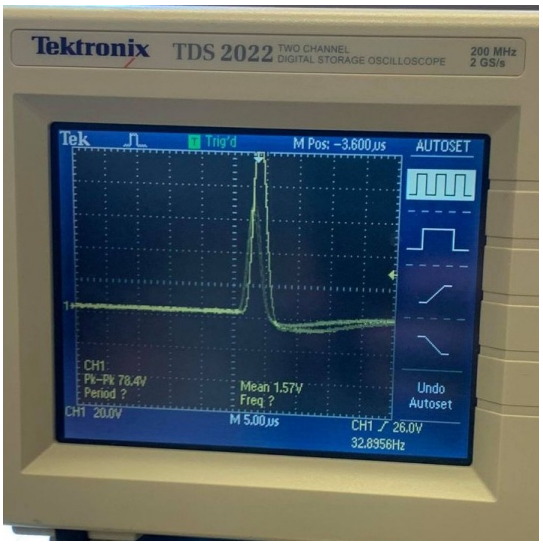

FIG. (5) Pulse signal after passing through the lin.amp. As seen, the linear amplifier inverts the polarity of the signal (by setting the "input" of the oscilloscope to negative). We also see the effect of shaping, where the dragging tail of the raw signal pulse in Fig.(4) has been shortened. This reduces the pile-up, thereby increasing the number of detected events and thus increasing the efficiency, as can be seen from Eq.(7).

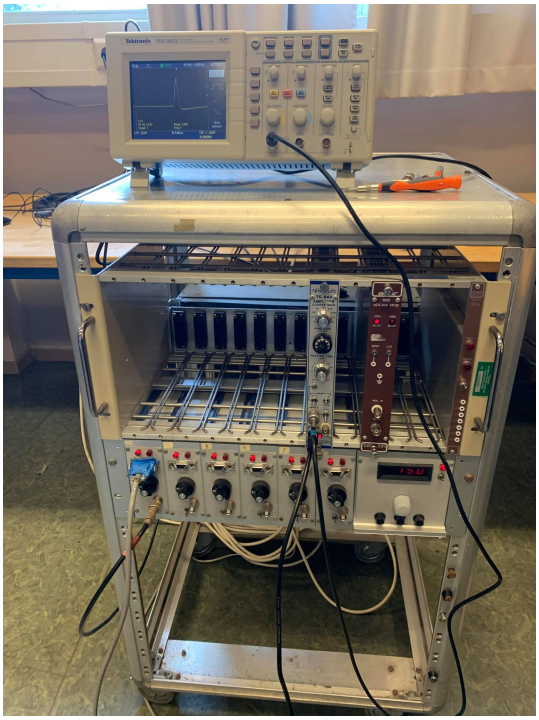

FIG. (6) Set-up of our signal processing equipment. On the bottom we se an array of voltage supplies. We connected to the first unit, and gradually increased the voltage to 750V. This is used to supply the bias voltage for the photomultiplier tube and other parts of our equipment. In the middle to the left, we see the linear amplifier in gray(Tennelec TC243). This box also serves as an Analog to digital converter (ADC). The now discretized signal is then sent to the MCA(Ortec 926-M-USB), which is seen to the right of the Tennelec. The histogram mentioned in Sec.(II) is then created and sent to the computer through a USB cable.

A data acquisition period of 5 minutes was used in sampling the various spectra. To be able to subtract the background from our signal+background spectra, we sampled the background radiation in addition to the Cesium and Cobalt sources. As will be seen in the coming sections, we only performed fits on the Cesium data sample. Results were therefore only obtained for this source, but could be obtained for Cobalt by use of the same statistical methods.

IV. Results and Discussion

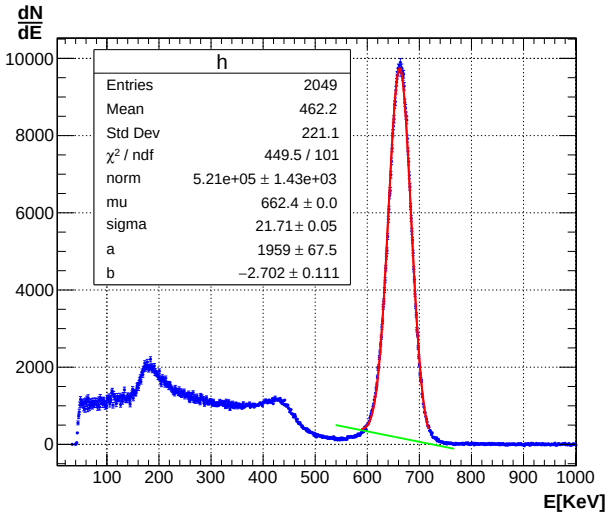

FIG. (8) Here we see the photopeak corresponding to Cesium decay. As seen, the peak was located at an energy of 662.4 keV ± 0.0 keV, which is slightly higher than the reference value of 661.7 keV. We also see that $^2/ndf$ = 449.5/101, a somewhat poor fit. As seen in the figure, this most likely stems from an upwards fluctuation in the data at the peak energy. The resolution of the photopeak was found calculated to be 7.71% ± 0.02%.

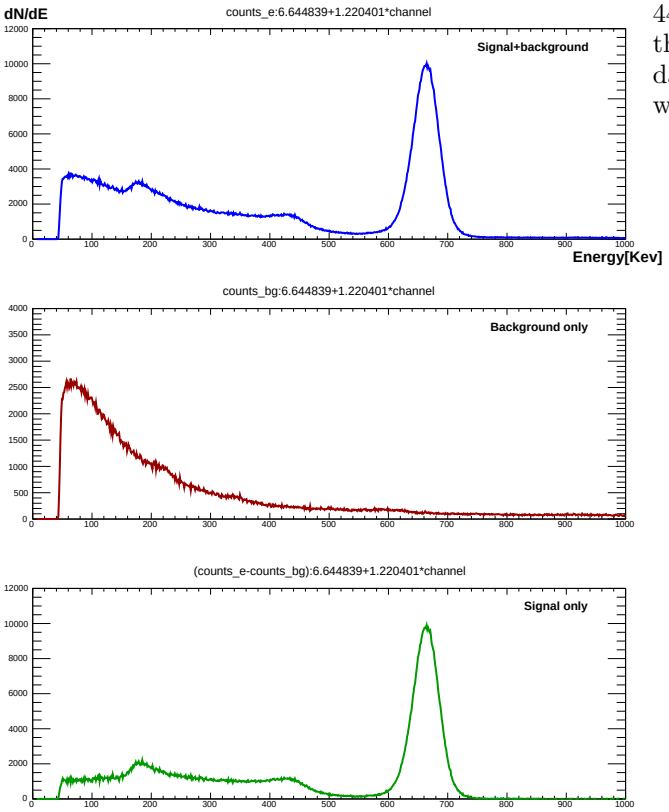

FIG. (7) In the first panel, we see the spectrum of the Cesium source + background. The second panel shows our data measurement for background only while the third panel is the result of subtracting the background from the signal+background spectrum. The the peak seen in the background spectrum stems from Potassium. We also have a contribution to the background from air showers produced by cosmic ray impacts in the atmosphere.

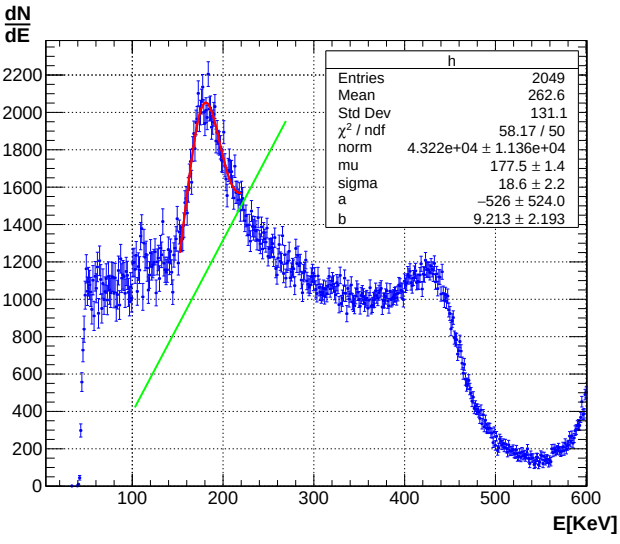

FIG. (9) Here we see the fit of the peak corresponding to Compton forward scattering ($\theta \approx 0$). As seen, its located at 177.5 keV ± 1.4 keV. Its resolution was found to be 24.2% ± 0 03%. Furthermore, we see that χ^2/ndf = 58.17/50 which is slightly above the expected value.

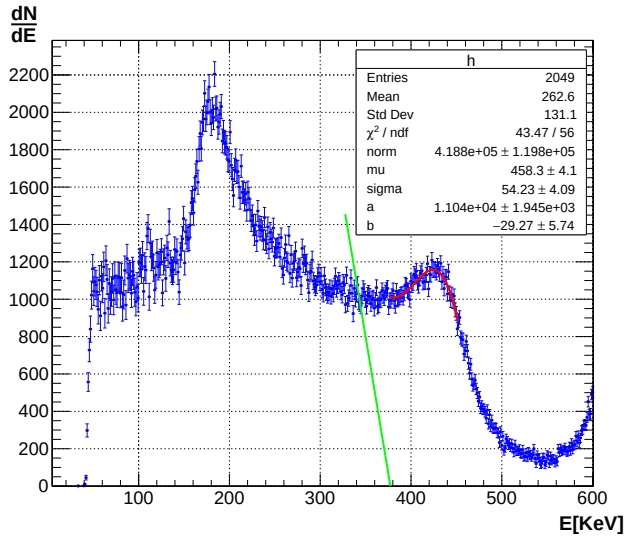

FIG. (10) Fit of the Compton backscattering peak($\theta = \pi$), i.e. the Compton edge. As seen, its energy was found to be 177.5 keV ± 1.4 keV. Its resolution was found to be 30.1% ± 0.02%. We also see that $\chi^2/ndf = 43.47/56$, indicating a better than expected fit.

TABLE (I) Fit results of the three peaks in our Cesium spectrum

Fit results			
	$^{137}_{55}$Cs peak	Compt($\theta = 0$)	Compt($\theta = \pi$)
Entries	2049	2049	2049
Mean	462.2	262.6	262.6
Std Dev	221.1	131.1	131.1
χ^2/ndf	449.5/101	58.17/50	43.47/56
norm	5.21e5 ± 1.43e3	4.322e4 ± 1.136e4	4.188e5 ± 1.198e5
μ	662.4 ± 0.0	177.5 ± 1.4	458.3 ± 4.1
σ	21.71 ± 0.05	18.6 ± 2.2	54.23 ± 4.09
a	1959 ± 67.5	-526 ± 524.0	1.104e4 ± 1.945e3
b	-2.702 ± 0.111	9.213 ± 2.193	-29.27 ± 5.74

TABLE (II) Resolution of the peaks in our Cesium spectrum

Peak properties			
	$^{137}_{55}$Cs peak	Compt($\theta = 0$)	Compt($\theta = \pi$)
E[keV]	662.4 ± 0.0	177.5 ± 1.4	458.3 ± 4.1
σ_E[keV]	21.71 ± 0.05	18.6 ± 2.2	54.23 ± 4.09
R[%]	7.72 ± 0.02	24.2 ± 0.03	30.1 ± 0.02

A. Resolution with uncertainty

As shown in Sec(II), the resolution of a peak is to a good approximation given by

$$R(\sigma, E) = \frac{2.35\sigma}{E} \tag{9}$$

Assuming that σ and E are independent variables, we can apply the error propagation formula in Eq.(8):

$$\begin{aligned}(\Delta R(\sigma,E))^2 &\approx (\Delta\sigma)^2 \left(\left.\frac{\partial R}{\partial\sigma}\right|_{\sigma,E}\right)^2 + (\Delta E)^2 \left(\left.\frac{\partial R}{\partial E}\right|_{\sigma,E}\right)^2 \\ &= (\Delta\sigma)^2 \left(\frac{2.35}{E}\right)^2 + (\Delta E)^2 \left(\frac{-2.35\sigma}{E^2}\right)^2\end{aligned} \tag{10}$$

Which is the expression we use to calculate ΔR in the script "calculate_res.C". σ and E with their associated uncertainties can be found in the Tab.(I) in the rows corresponding to σ and μ respectively.

B. Detector size

The size of the detector has a large impact the energy spectrum it produces for a given process.

For detectors that are much larger than the mean free path of gamma rays, of the order of tens of centimeters [1] , practically no gamma rays will escape from the crystal. The primary γ-ray may undergo a combination of Compton scattering and pair production, but all its energy will eventually be deposited to electrons in through photoelectric absorption. If the response of the detector is linear as a function of the these photoelectrons, then the detector response will always be the same for a γ-ray of a given energy. The spectrum produced is therefore a single peak at this energy, viz. the full-energy-peak.

For very small detectors 1-2 cm, practically all secondary γ-rays will escape the detector. Thus, the detector response will only be equal to the energy of the primary γ-ray ($h\nu$) in the case that it undergoes photoelectric absorption. In this case, we will observe a peak around around $h\nu$, aptly coined the photopeak. In the case of Compton scattering or pair production, the signal yield will be below this value due to part of the energy escaping the detector in the form of secondary photons. In our case, $h\nu < 2m_e c^2$ and so pair production cannot occur. The only contribution to our signal spectrum below the photopeak is therefore Compton scattering, as can be seen in Fig.(10).

Since it is the signal peak we're primarily interested in, we should therefore opt for as large of a detector as possible. However, such large detectors are not practical, and thus medium sized ones are often used.

In this case, the primary γ-ray may undergo Compton scattering multiple times or pair production followed by a number of Compton scatterings before escaping the detector. In both these cases, the energy response of the detector will be below the photopeak. In our case, we only have contribution from multiple Compton scatterings. Their contribution to the energy spectrum can be seen in Fig.(8). For a very small detector, there would be no signal between the Compton edge and the photopeak. However, due to multiple Compton scattering, a signal "valley" occurs. Multiple Compton scattering affects the whole Compton continuum and distorts it from the single scattering continuum on which our formulae are based.

C. Estimating the electron mass from the Compton edge

As shown in the appendix, the electron mass (in Natural units) is given by

$$E_r = 2E_i \frac{E_i - E_k(\theta = \pi)}{E_k(\theta = \pi)} \tag{11}$$

Here E_i is the energy of the incoming γ-ray and can be estimated from the energy of the photopeak, namely

- $E_i = 662.4 \pm 0.0$

E_k is the kinetic energy of the recoil electron for Compton scattering at $\theta = \pi$, and we estimate it from our fit to the Compton edge:

- $E_k(\theta = \pi) = 458.3 \pm 4.1$

Inserting this in Eq.(11) (and applying error propagation...) yields

$$E_r = 589.988 \tag{12}$$

Using $x = E_i$ and $y = E_k$ in Eq.8 and ignoring the Δx term since $\Delta E_i = 0.0$, we get

$$(\Delta E_r)^2 = (\Delta E_k)^2 \left(\frac{-2E_i^2}{E_k^2} \right)^2 \tag{13}$$

Which after insertion of the numerical values gives

$$\Delta E_r = 17.1\,\text{keV} \tag{14}$$

And thus our estimate of the electron rest mass is

$$E_r = 590.0\,\text{keV} \pm 17.1\,\text{keV} \tag{15}$$

This is quite a lot higher than the actual value of 511 keV which does not lie within our uncertainty (i.e. 68% CL interval). This discrepancy might be the assumptions made in deriving Eq.(11) coming back to haunt us. The real spectrum shown in Fig(10) is more complicated than the one for which Eq.(11) holds due to the following reasons:

- Multiple Compton scattering not only provides the curve observed between the Compton edge and the photopeak, but is also present at energies below the Compton edge, and distorts the single-scattering continuum on which Eq.(11) is based.
- Eq.(A.7) does not consider the binding energy of our electron, which leads to a "rounding" of the compton edge[1] and a general distortion of the continuum.
- The struck electron has angular momentum, which will result in a doppler spread in the Compton continuum around the energy of the incoming photon.

V. Conclusion

In this experiment, we measured the energy spectrum of ^{137}Cs by use of a Thallium activated Sodium iododie detector. By performing χ^2 fits to our data around the ^{137}Cs photopeak and the Compton edge, estimates of the energy of the γ-ray stemming from ^{137}Cs decay as well as the rest mass of the electron have been found.

These estimates were found to be $E_\gamma = 662.4\,\text{keV} \pm 0.0\,\text{keV}$ and $m_e = 590.0\,\text{keV} \pm 17.1\,\text{keV}$ respectively.

The resolution of all peaks in the spectrum were also calculated, of which the Photopeak and Compton edge are the most relevant. They were found to be $R_{\text{photopeak}} = 7.72\,\text{keV} \pm 0.02\,\text{keV}$ and $R_{\text{Compton edge}} = 30.1\,\text{keV} \pm 0.02\,\text{keV}$.

References

[1] Glenn F. Knoll. *Radiation Detection And Measurement.* 3rd ed. Wiley India Pvt. Ltd., 2009.

[2] William R. Leo. *Techniques for Nuclear and Particle Physics Experiments: A How-to Approach.* 2nd ed. Springer, 1994.

Appendices

A. χ^2 fitting

Let's assume we have a data set of consisting of n measurements, namely $\mathbf{n} = \{(x_1, y_1), (x_2, y_2), ..., (x_n, y_n)\}$, for which we wish to fit a curve. Below we see a depiction of the scatter plot of such a data set with a corresponding proposed fit curve, $h(x; \mathbf{a})$. Here $\mathbf{a} = \{a_1, a_2, ..., a_m\}$ are "shape parameters" which determine the functional form of this curve.

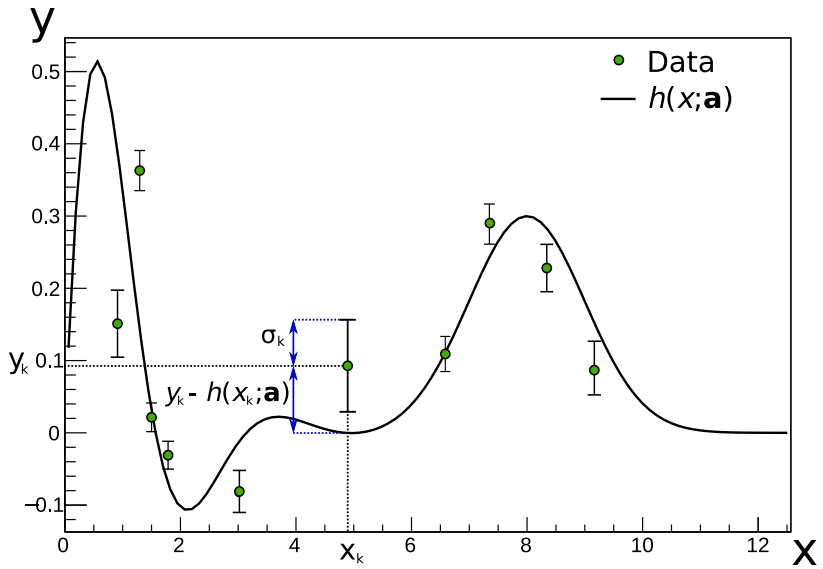

FIG. (11) Depiction of a scatter plot of a data set with a proposed fit curve.

When proposing a distribution, $h(x; \mathbf{a})$, we make the assumption that it is the true underlying distribution of the data set and calculate the χ^2 to see how well it fits our data. As we will see, the best fit is found when this χ^2 is as close to 0 as possible.

If the measured y values $\mathbf{y} = \{y_1, y_2, ..., y_n\}$ are i.i.d. according to a normal distribution with mean $\mu_i = h(x_i; \mathbf{a})$ and standard deviation σ_i, then their PDF is given by

$$f(\tilde{y}_i) = \frac{1}{\sqrt{2\pi\sigma_i^2}} \exp\left\{ -\frac{(\tilde{y}_i - h(x_i; \mathbf{a}))^2}{2\sigma_i^2} \right\} \tag{A.1}$$

Where $\tilde{y}_i$ is the stochastic variable from which we have "drawn" our measurement y_i. The likelihood function can be thought of as the joint PDF of our measurements. Since our measurements are i.i.d., we therefore have

$$L(\mathbf{a}; \mathbf{y}) = \prod_{i=1}^{n} f(\mathbf{a}; \tilde{y}_i = y_i) \tag{A.2}$$

Where we switched the order of the arguments to indicate that we are now holding the measurements fixed and considering the shape parameters $\mathbf{a}$ as our variables. Note that we don't include x_i in the arguments as they are uniquely determined by y_i.

We then proceed to maximize the likelihood[3] w.r.t. a. Since the logarithm is a strictly monotone function, this is equivalent to maximizing

[3] This corresponds to finding the functional form of the joint PDF from which it is most probable to that our data has been generated.

$$\ln L = \sum_{i=1}^{n} \ln f(\mathbf{a}; \tilde{y}_i = y_i) = -\frac{1}{2}\sum_{i=1}^{n} \ln\left(2\pi\sigma_i^2\right) - \frac{1}{2}\sum_{i=1}^{n} \frac{(y_i - h(\mathbf{a}; x_i))^2}{\sigma_i^2} \tag{A.3}$$

It is common to turn this into a minimization problem by multiplying both sides by -2;

$$-2\ln L = \sum_{i=1}^{n} \frac{(y_i - h(\mathbf{a}; x_i))^2}{\sigma_i^2} + \sum_{i=1}^{n} \ln\left(2\pi\sigma_i^2\right) \tag{A.4}$$

The standard deviations/errors of the measurements are fixed, and so the the last term in Eq.(A.4) can be ignored in our minimization/fitting procedure. The problem of finding the optimal parameters **a** for our fit curve has thus been transformed into finding the values of **a** which minimizes

$$\chi^2 \equiv \sum_{i=1}^{n} \frac{(y_i - h(\mathbf{a}; x_i))^2}{\sigma_i^2} \tag{A.5}$$

The quantity χ^2 will be distributed according to following PDF

$$f(\chi^2) = \frac{x^{n/2-1}}{2^{n/2}\Gamma(n/2)} e^{-x/2} \tag{A.6}$$

Which is the χ^2 distribution from which (perhaps confusingly) the χ^2 procedure takes its name. Here n is the number of degrees of freedom, which is just the number of terms in Eq.(A.5).

It can be shown that $E[f(\chi^2)] = n$.

A. Compton Scattering

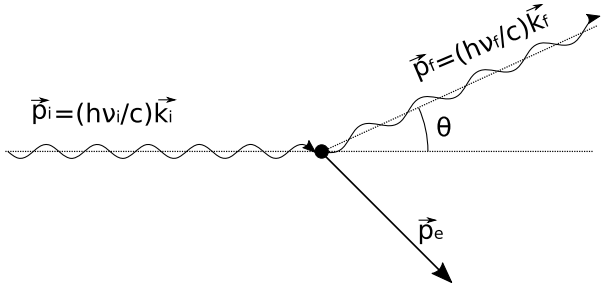

FIG. (12)

When a photon of sufficiently large energy strikes an electron of an atom, we can estimate the binding energy of this electron to be zero. In this case, **energy conservation** yields

$$h\nu_i + m_e c^2 = h\nu_f + \sqrt{m_e^2 c^4 + p_e^2 c^2} \tag{A.7}$$

$$\left(h(\nu_i - \nu_f) + m_e c^2\right)^2 = m_e^2 c^4 + p_e^2 c^2$$

$$\Rightarrow p_e^2 = \frac{h^2}{c^2}(\nu_i - \nu_f)^2 + 2h m_e(\nu_i - \nu_f) \tag{A.8}$$

From **momentum conservation**, we have

$$\begin{aligned}
\vec{p}_i &= \vec{p}_f + \vec{p}_e \\
\vec{p}_e \cdot \vec{p}_e &= (\vec{p}_i - \vec{p}_f) \cdot (\vec{p}_i - \vec{p}_f) \\
\Rightarrow p_e^2 &= \frac{h^2}{c^2}\nu_i^2 + \frac{h^2}{c^2}\nu_f^2 - 2\frac{h^2}{c^2}\nu_i\nu_f \cos\theta
\end{aligned} \tag{A.9}$$

Where we used $E^2 = m^2c^4 + p^2c^2 = p^2c^2$ for a massless photon. We thus have $p = \frac{E}{c} = \frac{h}{c}\nu$. In addition we used $\vec{p}_i \cdot \vec{p}_f = |\vec{p}_i||\vec{p}_f|\cos(\theta) = |\vec{p}_i||\vec{p}_f|\cos(-\theta) = \vec{p}_f \cdot \vec{p}_i$.
Setting Eq.(A.8) equal to Eq.(A.9) gives

$$\begin{aligned}
-2\frac{h^2}{c^2}\nu_i\nu_f + 2hm_e(\nu_i - \nu_f) &= 2\frac{h^2}{c^2}\nu_i\nu_f\cos\theta \\
-E_iE_f + m_ec^2(E_i - E_f) &= E_iE_f\cos\theta \\
m_ec^2(E_i - E_f) &= E_iE_f(1 - \cos\theta) \\
E_i &= E_f\left[\frac{E_i}{m_ec^2}(1 - \cos\theta) + 1\right] \\
\Rightarrow E_f &= \frac{E_i}{1 + \frac{E_i}{m_ec^2}(1 - \cos\theta)}
\end{aligned} \tag{A.10}$$

We are primarily interested in the kinetic energy of the recoiling electron, as this is what will cause scintillation in our NaI crystal. Denoting the rest mass m_ec^2 as E_r, we get

$$\begin{aligned}
E_i + E_r &= E_f + E_r + E_k \\
E_k &= E_i - E_f \\
E_k &= \frac{E_i\left(1 + \frac{E_i}{E_r}(1 - \cos\theta)\right)}{1 + \frac{E_i}{E_r}(1 - \cos\theta)} - \frac{E_i}{1 + \frac{E_i}{E_r}(1 - \cos\theta)} \\
E_k &= E_i\frac{\frac{E_i}{E_r}(1 - \cos\theta)}{1 + \frac{E_i}{E_r}(1 - \cos\theta)}
\end{aligned} \tag{A.11}$$

And so the kinetic energy of the recoil electron is given by

$$\boxed{E_k = E_i\frac{\tilde{E}_i(1 - \cos\theta)}{1 + \tilde{E}_i(1 - \cos\theta)}} \tag{A.12}$$

Where we defined $\tilde{E}_i \equiv \frac{E_i}{E_r}$.
In the case of backscattering, we have $\theta = \pi$ and so

$$E_k(\theta = \pi) = E_i\frac{2\tilde{E}_i}{1 + 2\tilde{E}_i} \tag{A.13}$$

From this we can also calculate the rest mass of the electron:

$$\begin{aligned}
E_k\big|_{\theta=\pi}\left(1 + 2\tilde{E}_i\right) &= 2E_i\tilde{E}_i \\
2\tilde{E}_i(E_k\big|_{\theta=\pi} - E_i) &= -E_k\big|_{\theta=\pi} \\
2\frac{E_i}{E_r}(E_i - E_k\big|_{\theta=\pi}) &= E_k\big|_{\theta=\pi} \\
E_r &= \frac{2E_i(E_i - E_k\big|_{\theta=\pi})}{E_k\big|_{\theta=\pi}}
\end{aligned} \tag{A.14}$$

The rest mass of the electron (in Natural units) is thus given by

$$\boxed{E_r = 2E_i \frac{E_i - E_k(\theta = \pi)}{E_k(\theta = \pi)}} \tag{A.15}$$